


NARRATIVE REVIEW

Open Access

# Virtual non-calcium dual-energy CT: clinical applications



Tommaso D'Angelo<sup>1</sup>, Moritz H. Albrecht<sup>2\*</sup> , Danilo Caudo<sup>1</sup>, Silvio Mazziotti<sup>1</sup>, Thomas J. Vogl<sup>2</sup>, Julian L. Wichmann<sup>2</sup>, Simon Martin<sup>2</sup>, Ibrahim Yel<sup>2</sup>, Giorgio Ascenti<sup>1</sup>, Vitali Koch<sup>2</sup>, Giuseppe Cicero<sup>1</sup>, Alfredo Blandino<sup>1</sup> and Christian Booz<sup>2</sup>

## Abstract

Dual-energy CT (DECT) has emerged into clinical routine as an imaging technique with unique postprocessing utilities that improve the evaluation of different body areas. The virtual non-calcium (VNCa) reconstruction algorithm has shown beneficial effects on the depiction of bone marrow pathologies such as bone marrow edema. Its main advantage is the ability to substantially increase the image contrast of structures that are usually covered with calcium mineral, such as calcified vessels or bone marrow, and to depict a large number of traumatic, inflammatory, infiltrative, and degenerative disorders affecting either the spine or the appendicular skeleton. Therefore, VNCa imaging represents another step forward for DECT to image conditions and disorders that usually require the use of more expensive and time-consuming techniques such as magnetic resonance imaging, positron emission tomography/CT, or bone scintigraphy. The aim of this review article is to explain the technical background of VNCa imaging, showcase its applicability in the different body regions, and provide an updated outlook on the clinical impact of this technique, which goes beyond the sole improvement in image quality.

**Keywords:** Algorithms, Bone marrow, Calcium, Edema, Tomography (x-ray, computed)

## Key points

- Virtual non-calcium (VNCa) computed tomography (CT) imaging provides new relevant clinical information compared to standard CT.
- VNCa improves CT sensitivity and specificity to assess bone marrow disorders.
- VNCa CT may serve as an alternative to magnetic resonance imaging in case of contraindications.

## Background

Since the advent of dual-energy computed tomography CT (DECT), numerous and noteworthy advantages over conventional CT have been investigated such as image optimization, artifact reduction, and the ability to

provide additional information regarding tissue composition [1–8].

Among different DECT applications, virtual non-calcium (VNCa) has become an increasingly popular technique due to its ability to subtract calcium from anatomical structures, resulting in better assessment of numerous pathological conditions that might be masked on standard CT. Firstly introduced in 2009, VNCa has found its mainstream applications in removing calcified plaques from vessels and depicting cancellous bone and bone marrow changes [9–13].

Bone marrow edema (BME) or “bone bruise,” is considered the biomarker of injury of the skeletal system and is associated with a reduction of fat component in the trabecular bone, replaced by edema and hemorrhage. Magnetic resonance imaging (MRI) represents the reference standard technique for the assessment of bone marrow disorders [14]. DECT may be considered a potentially cheaper, faster, and comprehensive imaging

\* Correspondence: [moritz.albrecht@kgu.de](mailto:moritz.albrecht@kgu.de)

<sup>2</sup>Division of Experimental Imaging, Department of Diagnostic and Interventional Radiology, University Hospital Frankfurt, Theodor-Stern-Kai 7, 60590 Frankfurt am Main, Germany  
Full list of author information is available at the end of the article

alternative through the creation of VNCA reconstructions, and it is aiming to provide as detailed information as MRI for a number of clinical indications [15].

A large body of evidence has shown the potential of DECT for collagen-based tendon and ligament imaging or to differentiate hyperdense lesions from calcium, such as urate crystals in patients with gout [16–20]. In this setting, DECT's ability to provide information regarding an additional imaging parameter such as BME derived from VNCA images might be particularly helpful for a multiparametric approach to inflammatory, infiltrative, and degenerative disorders as well as in an emergency setting for traumatized patients.

This article discusses and summarizes the current clinical applications of VNCA imaging including different DECT platforms, their basic principles of physics, and areas of potential development.

### Basic principles of DECT

While standard single-energy CT uses a single polychromatic x-ray beam with a single peak energy of 120 kV, DECT systems allow for simultaneous image acquisition at two different voltages.

At the energy levels used in clinical routine, attenuation of biological tissues is dependent on two major interactions: Compton scattering and photoelectric effects. Compton scattering is proportional to electron density and has little energy dependence. On the other hand, the photoelectric effect is dependent on the energy of the x-ray beam ( $E$ ), as well as on the atomic number ( $Z$ ) of the element, and it is predominant at lower energies and near the element K-edge.

On single-energy CT platforms, the measurement of attenuation using a single x-ray spectrum does not allow for the differentiation of materials, because the attenuation coefficient is not unique. In particular, it depends either on the energy of the x-ray beam or on the concentration of a material. This means that at a given energy, a lower concentration of a higher  $Z$  material (*i.e.*, iodine) may have the same attenuation as the higher concentration of a lower  $Z$  material (*i.e.*, calcium). However, since materials have unique attenuation profiles at different energy levels, DECT aims to identify different elements exploiting mathematical algorithms based on their linear attenuation coefficients in order to achieve the so-called *material decomposition* [21–23].

DECT's ability to discriminate between different materials is highly proportional to the dual-energy ratio ( $DE_{ratio}$ ). Since DECT uses two different energies for measuring attenuation,  $DE_{ratio}$  is defined as the ratio of the attenuation of a given material on a low-kV dataset to the attenuation of the same material on a high-kV dataset. The energy-dependent attenuation differences of elements within a voxel allow DECT to exploit two- and

three-material decomposition. The ability to differentiate the  $DE_{ratio}$  of two materials also depends on the separation between low- and high-energy spectra and the  $Z$  of the evaluated materials.

However, DECT algorithms work better when materials have high atomic numbers, because these are characterized by large differences in attenuation at different photon energies (*i.e.*, iodine and calcium). At tube voltages used in clinical routine, it is possible to generate virtual unenhanced images by subtraction of iodine from contrast-enhanced DECT examinations or VNCA series by subtraction of calcium [5, 15, 20, 24, 25].

Different vendors offer diverse DECT technologies:

- 1) *Dual-source CT (DSCT) platforms*, consisting of two x-ray tubes that generate two beams at different voltages installed at about 90° from each other, which have the advantage of high temporal resolution; although two x-ray sources are involved, the radiation dose administered to the patient is usually divided between the two, resulting in dose neutrality of second- and third-generation DSCT scanners compared with conventional CT [25, 26];
- 2) *Single-source with sequential acquisition CT platforms*, which consist of two scans acquired consecutively at different tube potentials followed by co-registration for post-processing, offering the advantage of a full field of view and the drawback of poor temporal resolution as the patient is scanned twice, with an increase of radiation dose;
- 3) *Single-source twin-beam platforms*, in which a two-material filter splits the x-ray beam into high- and low-energy spectra on the  $z$ -axis before it reaches the patient;
- 4) *Single-source tube voltage switching CT platforms*, in which the x-ray tube alternates high and low potentials several times within the same rotation, which have the advantage of a full field of view;
- 5) *Dual-layer detector CT platforms*, which involve a superficial and a deep layer within the same detector plate that simultaneously collect low-energy data by the superficial layer, and high-energy data by the deep layer.

However, most of the current experience with VNCA algorithms published in scientific literature has been performed on second- and third-generation DSCT platforms (Tables 1, 2, 3, and 4), which may be explained with wider availability of this particular DECT technology compared to the other ones.

### Technical background of VNCA CT imaging

Due to three-material decomposition, the VNCA algorithm estimates the amount of calcium on the DECT

**Table 1** Virtual non-calcium computed tomography (CT) ability to differentiate hemorrhage from parenchymal calcifications on dual-energy head scans

Authors, year [reference]	DECT platform	Study type	Qualitative analysis (sensitivity, specificity, accuracy)	Quantitative analysis cutoff (sensitivity, specificity, accuracy)	Reference standard
Wiggins et al., 2019 [19]	DSCT	Clinical (137 patients)	100%, 100%, 100%	44 HU (100%, 93%, 95%)	MRI
Hu et al., 2016 [17]	DSCT	Clinical (62 patients)	96%, 100%, 99%	NA	MRI or clinical follow-up
Nute et al., 2015 [18]	VSCT	Phantom	NA	50 HU (NA, NA, 90%)	MRI

DECT Dual-energy computed tomography, DSCT, Dual-source CT, HU Hounsfield units, MRI Magnetic resonance imaging, NA Not available, VSCT Voltage-switching CT

dataset and subtracts it from images to highlight the anatomical structures that can be covered with bone mineral or gross calcifications.

On VNCA imaging, the bone marrow attenuation represents CT values of yellow and red marrow. In particular, using the characteristic slope of the  $DE_{ratio}$  of calcium, bone mineral voxels are projected to the CT value of water (0 HU for both 100 kV and Sn140 kV) [27, 28]. As a consequence, the differences among voxels reflect mainly the water and fat content in the bone marrow. These differences can be visually interpreted, using color-coded maps, or quantitatively assessed by means of regions of interest and expressed in HU [22, 29–31].

However, most of the cutoff values that have been suggested to differentiate BME from normal bone marrow are still quite heterogeneous, and range between -80 and 6 HU. These differences might depend either on the anatomical region evaluated or on the type of DECT platform used.

Image quality on VNCA datasets is also influenced by DECT scanning parameters. The use of higher spectral

separation allows for a precise assessment of bone mineral content [32]. Best results have been obtained with a  $DE_{ratio}$  of 70/150 kV. However, when a wide  $DE_{ratio}$  may not be recommended because of the increase in image noise, such as scanning the abdomen and pelvis, higher radiation doses help provide optimal image quality [31]. Pitch and rotation time do not considerably affect image quality, although spiral artifacts can appear when the pitch is too low.

Color-coded VNCA datasets are usually automatically processed from raw data of most modern DECT platforms, with processing time lasting few minutes, and showing the potential to be used in routine clinical practice [33, 34]. Slice thickness of 1–2 mm and smoother reconstruction kernels are recommended and datasets should be reformatted along two anatomical planes for optimal qualitative evaluation [35].

Technical limitations of VNCA imaging should also be taken into account. In fact, it has been demonstrated the inability to accurately visualize minor alterations in marrow attenuation directly adjacent to cortical bone due to incomplete masking of the cortex and to spatial

**Table 2** Virtual non-calcium computed tomography (CT) ability to depict traumatic bone marrow edema on dual-energy spine scans

Authors, year [reference]	DECT platform	Number of patients	Qualitative analysis (sensitivity, specificity, accuracy)	Quantitative analysis cutoff (sensitivity, specificity, accuracy)	Reference standard	Spine site
Wang et al., 2020 [51]	DSCT	20	85%, 97%, 93%	-12 HU (95%, 86%, 98%)	MRI	T/L
Jeong et al., 2020 [52]	DSCT	31	83%, 99%, 99%	NA	MRI	T/L
Booz et al., 2020 [29]	DSCT	52	93%, 95%, 90%	-43 HU (85%, 95%, 97%)	MRI	S
Foti et al., 2019 [58]	DSCT	76	88%, 92%, 90%	cutoff NA (92%, 90%, 91%)	MRI	T/L
Diekhoff et al., 2019 [53]	SACT	70	72%, 70%, NA	NA	MRI	T/L
Frellessen et al., 2018 [45]	DSCT	51	96%, 96%, 98%	NA	MRI	T/L
Diekhoff et al., 2017 [57]	SACT	9	88%, 100%, NA	NA	MRI	T/L
Petritsch et al., 2017 [54]	DSCT	22	64%, 99%, 93%	-47 HU (92%, 82%, 84%)	MRI	L
Kaup et al., 2016 [55]	DSCT	49	90%, 90%, 95%	NA	MRI	T/L
Bierry et al., 2014 [10]	DSCT	20	84%, 97%, 95%	cutoff NA (85%, 82%, NA)	MRI	T/L
Wang et al., 2013 [27]	DSCT	63	NA	-80 HU (96%, 98%, 97%)	MRI	T/L

DECT Dual-energy computed tomography, DSCT Dual-source computed tomography, SACT Sequential acquisition computed tomography, HU Hounsfield units, NA Not available, MRI Magnetic resonance imaging, T Thoracic, L Lumbar, S Sacral

**Table 3** Virtual non-calcium computed tomography potential to visualize non-traumatic bone marrow edema on dual-energy scans of spine and pelvic girdle

Authors, year [reference]	DECT platform	Number of patients	Qualitative analysis (sensitivity, specificity, accuracy)	Quantitative analysis cutoff (sensitivity, specificity, accuracy)	Reference standard	Disorder	Anatomical site
Shinohara et al., 2020 [61]	DSCT	53	NA	NA	MRI	Disc degeneration	Spine
Foti et al., 2020 [74]	DSCT	59	95%, 86%, 93%	NA	MRI	Sacroiliitis	Hip
Chen et al., 2020 [71]	DSCT	40	81%, 94%, NA	-44 HU (76%, 91%, NA)	MRI	Sacroiliitis	Hip
Gruggeberger et al., 2020 [73]	DSCT	47	93%, 94%, NA	-35 HU (94%, 83%, NA)	MRI	Sacroiliitis	Hip
Abdullayev et al., 2019 [56]	DLCT	21	85%, 84%, 84%	NA	MRI	Vertebral metastases	Spine
Booz et al., 2019 [34]	DSCT	41	91%, 92%, 94%	NA	MRI	Disc herniation	Spine
Wu et al., 2019 [70]	DSCT	47	93%, 94%, 92%	-33 HU (90%, 83%, 83%)	MRI	Sacroiliitis Spondylarthritis	Spine/Hip
Kosmala et al., 2018 [12]	DSCT	53	NA	-36 HU (100%, 97%, 99%)	MRI	Multiple myeloma	Spine
Kosmala et al., 2018 [66]	DSCT	34	91%, 91%, 91%	-45 HU (93%, 92%, 93%)	MRI	Multiple Myeloma	Spine

DECT Dual-energy computed tomography, DLCT Dual-layer computed tomography, DSCT Dual-source computed tomography, HU Hounsfield units, NA Not available, MRI Magnetic resonance imaging

averaging. Incomplete subtraction of cortical or cancellous bone might also occur in the case of arthrosis, and in the presence of gas or severe osteosclerosis, which causes beam hardening artifacts that may result in a lack of visible edema even in the presence of a fracture. For this reason, any potential user of VNCa imaging should be aware of its potential pitfalls [36, 37].

## VNCa clinical applications

### Head

Intracranial calcifications are common findings on head CT scans [38]. They are often caused by dystrophic processes within the choroid plexus and basal ganglia or might occur as part of different disorders, such as tuberous sclerosis, cysticercosis, Sturge-Weber syndrome, and

**Table 4** Virtual non-calcium computed tomography ability to depict traumatic bone marrow edema on dual-energy scans of appendicular skeleton

Author	DECT platform	Number of patients	Qualitative analysis (sensitivity, specificity, accuracy)	Quantitative analysis cutoff (sensitivity, specificity, accuracy)	Reference standard	Anatomical site
Yang et al., 2020 [81]	DSCT	156	92%, 93%, 93%	NA	MRI	Knee
Booz et al., 2020 [82]	DSCT	56	96%, 97%, 97%	-51 HU* (96%, 97%, 96%)	MRI	Knee
Yadav et al., 2020 [83]	DSCT	40	94%, 91%, 92%	NA	MRI	Lower limb
Wang et al., 2019 [80]	DSCT	35	88%, 98%, 95%	-67 HU (81%, 99%, 90%)	MRI	Knee
Booz et al., 2019 [85]	DSCT	62	92%, 97%, 98%	-53 HU (82%, 95%, 98%)	MRI	Calcaneus
Foti et al., 2019 [87]	DSCT	40	92%, 86%, 90%	-20 HU (88%, 92%, 87%)	MRI	Ankle
Jang et al., 2019 [36]	DSCT	35	100%, 100%, 100%	-55 HU (100%, 94%, 95%)	Standard CT	Hip
Ali et al., 2018 [86]	DSCT	24	NA	6 HU (100%, 99%, 100%)	Visual assessment	Wrist
Kellock et al., 2017 [37]	DSCT	118	100%, 100%, NA	NA	Clinical follow-up	Hip
Reddy et al., 2015 [69]	DSCT	25	90%, 40%, NA	NA	Clinical follow-up	Hip
Guggenberger et al., 2012 [47]	DSCT	30	90%, 81%, 97%	NA	MRI	Ankle

BME Bone marrow edema, CT Computed tomography, DECT Dual-energy computed tomography, DSCT Dual-source computed tomography, HU Hounsfield units; NA Not available, MRI Magnetic resonance imaging. \*Cutoff value refers to tibial BME

slowly growing brain tumors (*i.e.*, meningiomas, dermoids, craniopharyngiomas, and oligodendrogliomas) [39].

In an emergency setting, any focal source of intracranial hyperattenuation might confound diagnosis, especially if intracranial hemorrhage needs to be excluded. In a conventional CT scan of the head, any lesion with attenuation levels greater than 100 HU is classified as a calcification [40]. However, fresh blood usually has a density of 50–65 HU whereas attenuation of calcifications can vary between 70 and 200 HU [41]. Hence, this standard criterion may fail for lesions with attenuation levels inferior to 100 HU, where values tend to overlap.

Currently, the proposed imaging techniques for differentiating hemorrhage from calcification include MRI-based techniques such as quantitative susceptibility mapping and gradient-echo imaging [40].

VNCa has been shown to accurately differentiate between calcification and hemorrhage, even in lesions with attenuation comprised between 50 and 100 HU (Fig. 1) [18]. In clinical studies, VNCa with a cutoff of 44 HU has shown high diagnostic performance for differentiation of small foci of intracranial hemorrhage from calcium (Table 1) [17, 19].

## Spine

### Fractures

MRI and CT are currently considered the diagnostic imaging modalities of choice to evaluate spine disorders [42]. CT imaging is indicated in emergency trauma settings to detect hypodense fracture lines due to its excellent spatial resolution [42, 43]. On the other hand, MRI is the reference standard technique for the evaluation of

nerves, musculotendinous structures, and bone marrow disorders. Moreover, MRI is particularly useful to diagnose BME secondary to trauma, which allows establishing the chronicity of a fracture by the presence of interstitial fluid [44–46]. However, MRI access can be limited in routine trauma settings due to its high costs and long acquisition times, which require prolonged and potentially painful patient positioning [32, 46–48].

While single-energy CT is not able to remove bone trabeculations and to uncover subtle bone marrow attenuation changes, DECT allows for BME assessment [20, 49–55]. Moreover, its rapid acquisition time lends it favorably to emergency settings [46]. Several studies have been carried out to evaluate the diagnostic performance of VNCa reconstructions to detect acute vertebral fractures [56–58]. BME detection has been qualitatively assessed by using color-coded images and quantitatively using region-of-interest-based measurements of bone marrow attenuation. When microfractures are present within the cancellous bone, bone marrow attenuation increases since its fatty content is replaced by edema and microhemorrhages. Color-coded VNCa reconstructions show good to excellent results for qualitative assessment of BME, either in terms of sensitivity (range 72–96%), specificity (range 70–100%), and accuracy (range: 90–99%) (Table 2).

Similarly, receiver operating characteristic curve analysis of bone marrow attenuation on VNCa datasets has also demonstrated excellent sensitivity, specificity, and accuracy, ranging 85–96%, 82–90%, and 85–91%, respectively, using cutoff values from -80 and -12 HU [46, 56–58].

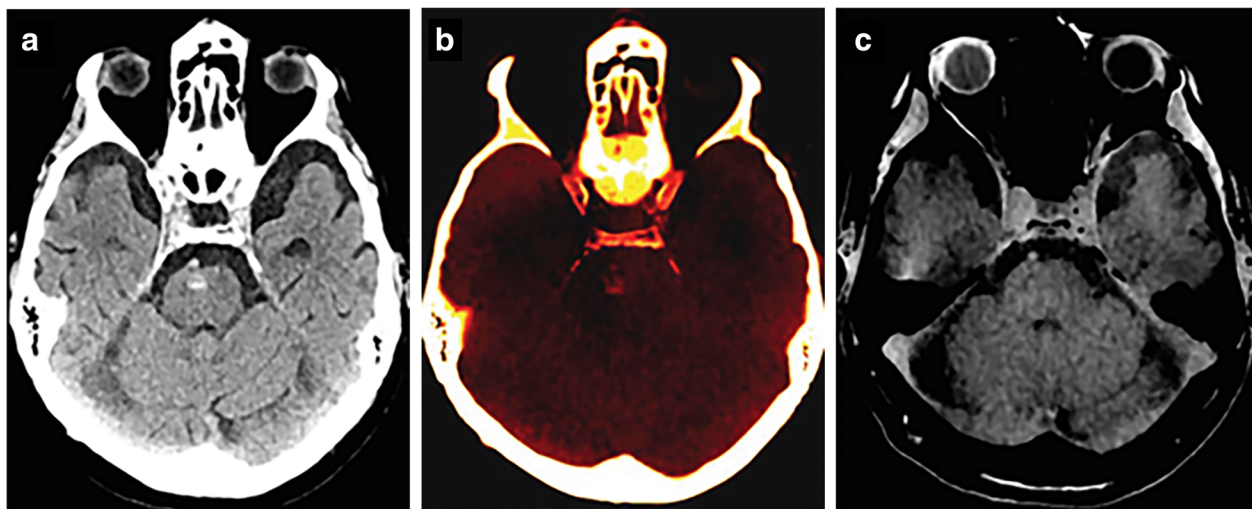


**Fig. 1** Head dual-energy computed tomography scan shows a focal hyperattenuation in the pons classified as indeterminate at standard grayscale series (a). This 80-year-old patient with a history of hypertension presented to the emergency department with altered mental status. On the calcium-overlay image (b), the hyperattenuation focus remains visible, while it is not apparent on the virtual non-calcium image (c), suggestive for parenchymal calcification. The finding was confirmed by magnetic resonance imaging. From Hu et al. [17]

Interesting results have also been obtained for the diagnosis of sacral insufficiency fractures (Fig. 2), showing high sensitivity and specificity (93% and 95%, respectively) for qualitative assessment, and values of 85% and 95% for quantitative assessment using a cutoff value of -43 HU [29]. This may allow DECT to act as a promising technique to avoid misinterpretation of insufficiency fractures and their related complications, particularly in patients suffering from osteoporosis or diffuse bone disease [59].

#### **Degenerative disc disease**

Degenerative disease of intervertebral disc apparatus is a common age-related condition, causing lower back pain and entailing substantial social and economic burden [34].

Common complications are compressions of the spinal cord or spinal nerve root. Fast and accurate diagnosis is necessary for rapid initiation of optimal therapy and to avoid compressions that can result in irreversible morbidity. MRI is the preferred diagnostic imaging modality due to its ability to provide excellent demarcation between the intervertebral disc and cerebrospinal fluid [60]. However, MRI has several limitations in clinical routine, such as patients with ferromagnetic metallic implants, claustrophobia, or difficulties in staying supine and still for long acquisition times.

DECT imaging has been introduced as an attractive alternative, especially due to VNCA imaging, which achieved promising results for the identification of early stages of intervertebral disc degeneration. Using a maximum CT value of 800 HU and a threshold of -200 HU, VNCA color-coded maps with mixed CT overlay have demonstrated the ability to detect different grades of the

modified Pfirrmann classification, which is widely used for disc degeneration grading [61]. In particular, VNCA imaging is able to detect an increase in disc attenuation that positively correlates to dehydration of nucleus pulposus and in a loss of its proteoglycan and water content.

More advanced stages of intervertebral disc degeneration are characterized by disc height reduction, fissuration of the annulus fibrosus, and herniation of the nucleus pulposus. Standard CT has shown moderate sensitivity and specificity for the detection of lumbar disk herniation, despite the improved results coming from new iterative reconstruction algorithms [34, 62, 63]. More recently, DECT has overcome the impaired contrast resolution of intervertebral discs by application of color-coded VNCA reconstructions (Fig. 3).

Color-coded maps help distinguish small disc herniations from cerebrospinal fluid, with better sensitivity and specificity compared to standard CT, respectively of 91% and 92%, using MRI as a reference standard (Table 3) [34].

#### **Infiltrative disease**

The spine represents the most common site of bone metastases. Only breast, prostate and lung cancers are together responsible for more than 80% of cases of metastatic bone disease [64].

A contrast-enhanced CT scan is typically performed in oncologic patients either for staging and follow-up purposes [56]. However, despite iodine-based contrast agents helping enhance soft tissue contrast, the assessment of bone lesions on standard CT remains challenging. In a meta-analysis, conventional CT images reported a sensitivity and specificity of 77% and 83% for

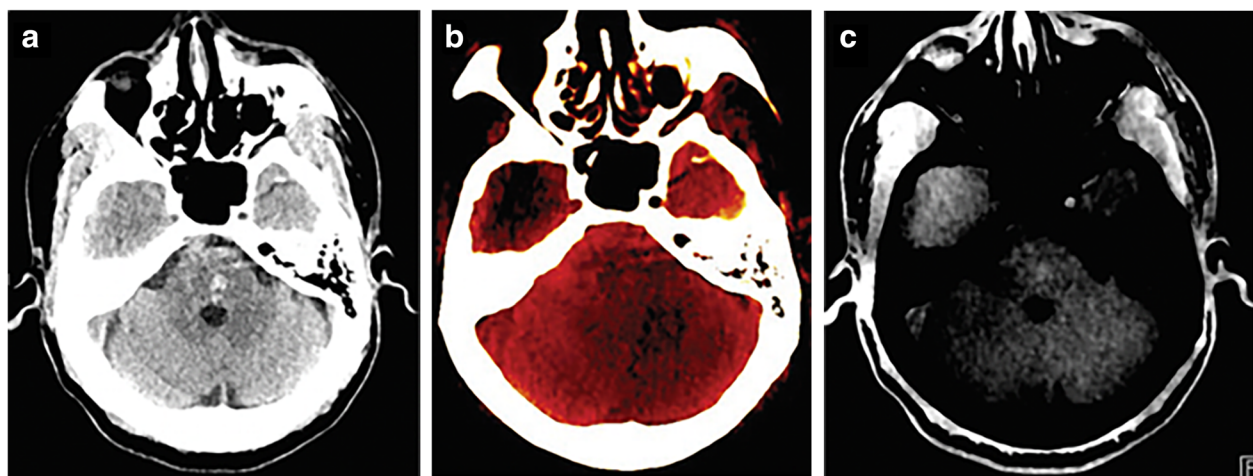


**Fig. 2** Head dual-energy computed tomography scan shows focal hyperattenuation in the pons, classified as indeterminate at standard grayscale series (a). This 58-year-old patient had a history of hypertension and diabetes and presented to the emergency department with right arm tremor, blurry vision, and increased systolic blood pressure. On the calcium-overlay image, the focal hyperattenuation in the pons was not apparent (b). On the virtual non-calcium image (c), the focal hyperattenuation in the pons manifests as a focal area of high attenuation, compatible with hemorrhage. From Hu et al. [17]

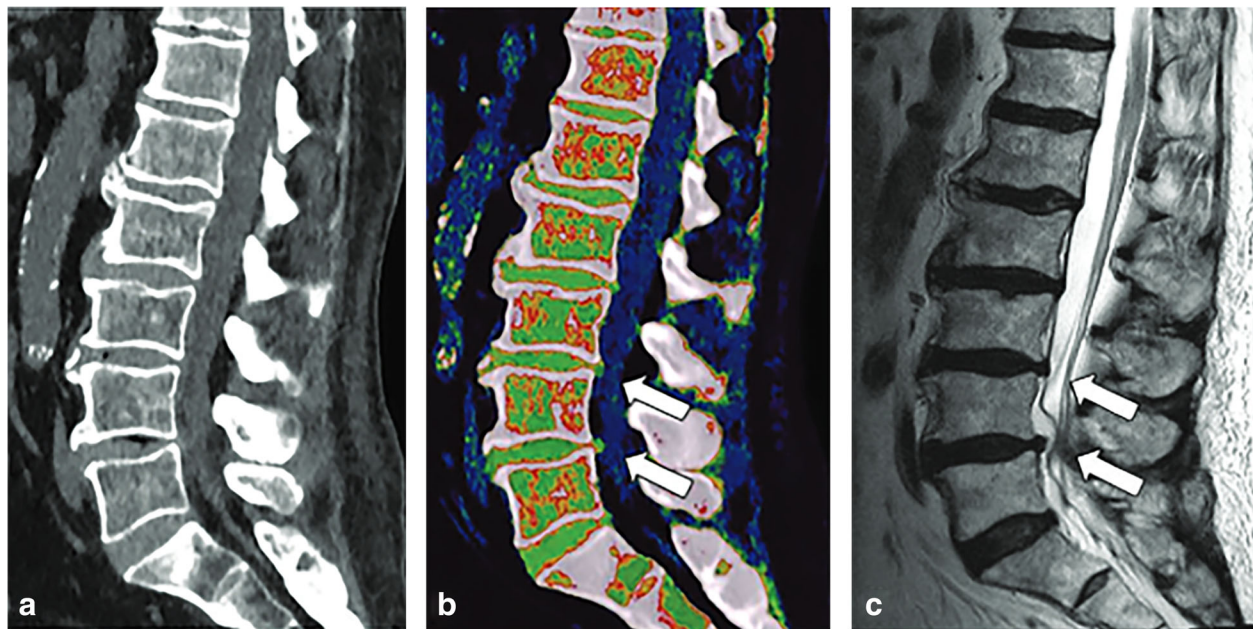


**Fig. 3** Spine dual-energy computed tomography. Standard grayscale series (a) shows typical findings of spondylarthrosis with vacuum phenomena in L3/L4 and L4/L5 intervertebral discs. Virtual non-calcium reconstruction with optimization for intervertebral disc analysis (b) can finely show the protrusion of lumbar discs (arrows), confirmed by magnetic resonance imaging T2-weighted sequence (c) (arrows). From Booz et al. [34]

detection of spine metastasis [65]. Moreover, patients may need to undergo additional imaging techniques, such as MRI, scintigraphy, or positron emission tomography when there is high suspicion for bone metastasis presence [56].

The efficacy of VNCA reconstructions to detect metastatic spine lesions has been recently assessed with different calcium suppression indices. In particular, the use of low- and medium-suppression indices resulted in an increase in sensitivity to 85%, compared to 78% of conventional CT, and it was associated with a good inter-reader agreement at subjective image analysis [56].

In a study from Abdullayev et al. [56], quantitative analysis using low- and medium-suppression indices showed promising results to discriminate between normal and metastatic bone, using a cutoff of -143 HU and -31 HU, respectively (Table 3).

The role of DECT in infiltrative spine disorders has also been focused on patients with multiple myeloma. In this malignant hematological tumor, the unbridled clonal proliferation of plasma cells causes an alteration of the normal components of bone marrow [66]. Low-dose total body CT scans are usually performed to detect osteolytic lesions [66]. In this setting, DECT has shown promising results, with better sensitivity compared to standard CT (Fig. 4).

Different studies have proposed threshold values ranging between -45 HU and -36 HU to achieve optimal

sensitivity by quantitative assessment and to allow fine depiction either of focal and diffuse patterns of disease, with accuracy ranging from 93 to 99% [12, 66, 67].

### Appendicular skeleton

#### Hip

VNCA reconstructions are particularly helpful to detect subtle hip fractures that might be missed on conventional radiographs or standard CT, especially in patients affected by diffuse skeletal disorders such as osteoporosis or Paget's disease [36].

Prompt identification of pelvic fractures is crucial for therapeutical planning and misdiagnosis is related to disability and higher mortality rates, with complications such as avascular necrosis and thromboembolism [68]. Different authors focused on the diagnostic performance of VNCA reconstructions to detect pelvic fractures, using clinical follow-up as a reference standard (Table 3). In these studies, DECT performed significantly better than standard CT, showing an improvement of sensitivity (> 5%) when color-coded VNCA images were evaluated [37, 69]. Moreover, quantitative analysis with a cutoff of -55.3 HU yielded sensitivity and specificity of 100% and 94%, respectively [36].

Different conditions such as axial spondylarthritis and sacroiliitis, involving either the spine or the pelvic girdle, usually require patients to undergo MRI. The VNCA algorithm has also been investigated for inflammatory

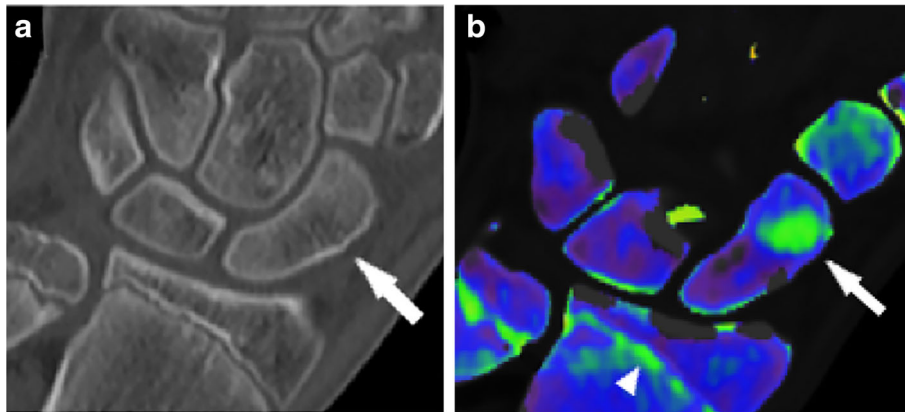


**Fig. 4** Hand dual-energy computed tomography scan in a patient with a non-displaced scaphoid fracture, which was confirmed at magnetic resonance imaging (not shown). Standard grayscale series (**a**) shows a subtle cortical interruption, which is not clearly suggestive for fracture (arrow). Color-coded virtual non-calcium image (**b**) depicts the presence of bone marrow edema confirming the hypothesis of a traumatic lesion. Of note, the epiphyseal line on the distal radius and ulna are also color-coded in green (arrowhead). From Dareez et al. [84]

changes of the bone marrow (Table 3), with results showing good diagnostic performance to highlight BME caused by active inflammation [70–74]. Promising results have also been shown for infiltrative lesions, and VNCA has been used as a guide for biopsy of malignant pelvic neoplasms that are barely visible on standard CT because of isodense bone marrow [75].

### Limbs

A recent meta-analysis [76] compared the diagnostic performance of CT and MRI to establish a definitive diagnosis of a suspected fracture in small bones. MRI yielded superior sensitivity and specificity compared to CT (respectively 88% and 100% versus 72% and 99%), using bone scintigraphy as a reference standard. In case of suspected or subtle fractures, MRI is considered the best advanced imaging option after conventional radiography, as it finely depicts bone marrow and adjacent soft tissues. On the other hand, MRI alone may not depict fracture lines in case of intense BME, and conventional radiographs or CT may be needed for diagnosis [77]. Additionally, high cost, low access, and contraindications prevent MRI from playing a role as an advanced imaging option for suspected and occult fractures in emergency settings [76, 78]. However, bone bruise is considered the key finding of bone injury at MRI, as it allows uncovering subtle fractures even in small bones that might be occult at conventional radiography and standard CT [79].

An increasing number of studies have shown the feasibility of DECT to detect traumatic BME in small bones of appendicular skeleton exploiting VNCA imaging (Table 4), with improved diagnostic performance compared to standard CT either for qualitative and quantitative evaluation [80–83].

DECT can complement the information provided by standard CT imaging and enhance the diagnostic capabilities of VNCA for the evaluation of acute knee fractures (Fig. 5). In a study by Booz et al. [82], qualitative assessment of knee fractures by color-coded VNCA images yielded sensitivity and specificity of 95%, while at quantitative analysis, these values were 96% and 97%, respectively, using a -51 HU cutoff. Similar results have been shown by Wang et al. [80], who proposed a cutoff of -67 HU, yielding a sensitivity of 81% and specificity of 99%. Compared with standard CT, DECT has demonstrated a 15–20% increase in sensitivity to detect fractures, especially for less experienced radiologists [81]. The VNCA algorithm has been shown to perform well even with a low radiation-dose protocol, with excellent agreement with standard-dose DECT [48]. Bipartite patella and osteoarthritis can represent a pitfall of the VNCA algorithm, since they may determine false positives and negatives [81]. An additional limitation represents also the presence of prostheses or osteosynthesis implants [81].

Several authors have investigated the performance of VNCA reconstructions to detect traumatic BME in small bones of distal joints, such as the scaphoid [47, 84–88]. In these studies, DECT was able to highlight traumatic BME with higher sensitivity and specificity than standard CT either for qualitative assessment and quantitative analysis (Table 4) [85]. Some case reports also highlighted the ability of DECT to depict Achilles tendon tears with improved confidence over conventional CT [89]. Similar outcomes have been reported for evaluation of cruciate ligament rupture in acute knee trauma, with rather good sensitivity (79%) and excellent specificity (100%), using MRI as a reference standard [16].



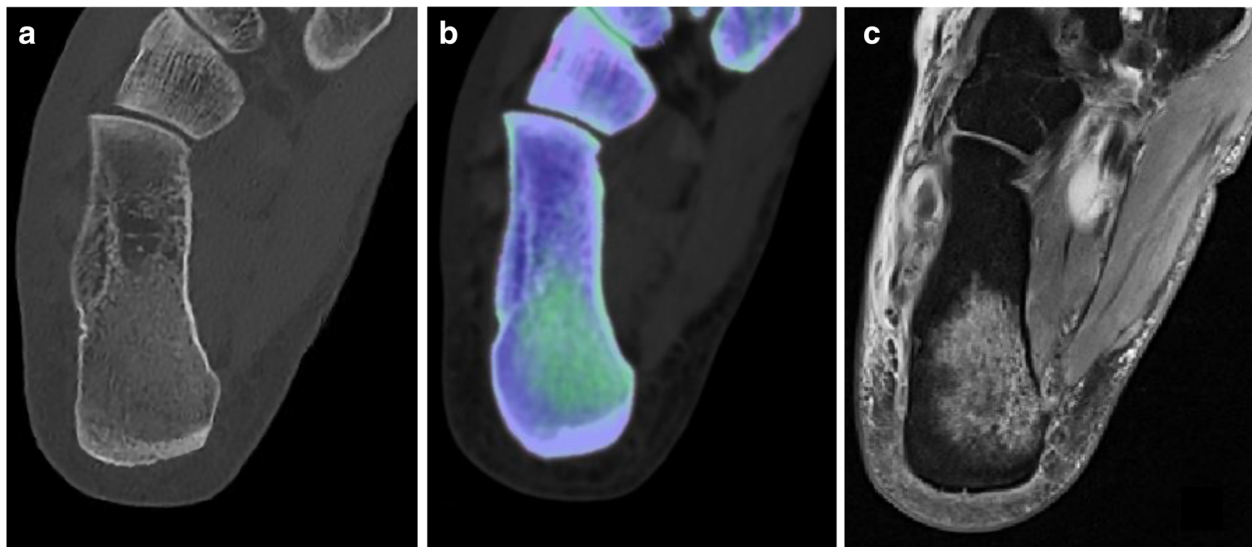


**Fig. 5** Dual-energy computed tomography scan in a patient presenting with right-sided acute ankle trauma. Standard grayscale series (a) does not depict any fracture line. Color-coded virtual non-calcium image (b) shows a distinct traumatic bone marrow edema of the right calcaneus, displayed as a green area (arrow). The finding was confirmed by magnetic resonance imaging (c) using a proton density-weighted sequence (arrow)

VNCA imaging performs well on small bones also to depict inflammatory BME, related to rheumatoid arthritis, in either large or small joints (Fig. 6), showing good qualitative assessment and excellent agreement with MRI [72].

### Vascular applications

Sufficient removal of calcified plaques from vessels represents a current challenge for CT angiography (CTA) studies. Calcified plaques commonly cause overestimation of vascular stenosis assessment, especially in

small vessels, and may lead to unnecessary invasive procedures [90].

Usually, a fixed HU value is used as a threshold to remove calcifications in conventional CTA, despite this method often failing due to calcium blooming. Alternatively, unenhanced CT acquisition can serve as a mask for subtraction of calcified plaques. However, misregistration artifacts may occur due to patient's movements or arterial pulsations between the two scans [13, 91]. DECT algorithms are well known to improve image quality, to reduce the contrast medium volume and the radiation dose to patients undergoing CTA studies [6,

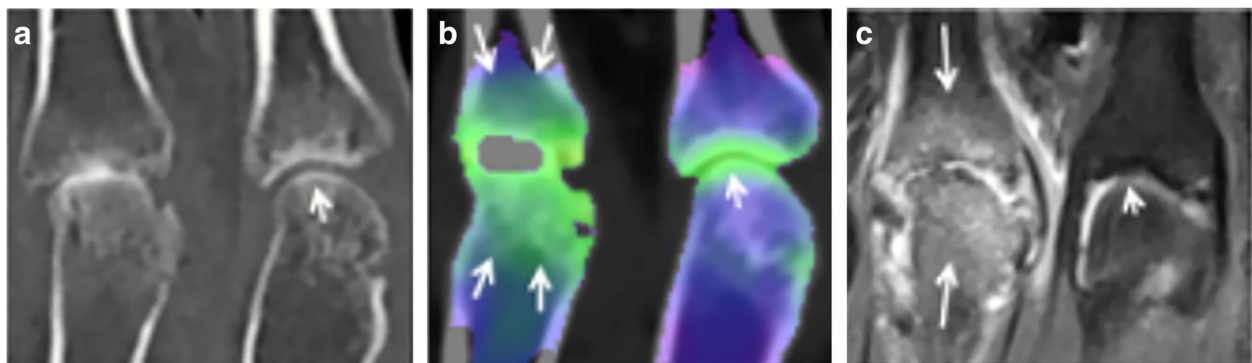


**Fig. 6** Dual-energy computed tomography scan of hands in a patient with rheumatoid arthritis. Magnification on the second metacarpophalangeal joint shows a normal and smooth outline of cartilage and bone plate (short arrows) on standard grayscale series (a) and normal virtual non-calcium attenuation (b). Conversely, bone marrow edema is evident on the third metacarpophalangeal joint presenting as an extensive and ill-defined green area (long arrows). Magnetic resonance imaging by means of T2-weighted fat-saturation sequence confirmed the presence of inflammatory bone marrow edema (c). From Jans et al. [72]

13, 92–94]. DECT-based three-material decomposition also allows for subtraction of the calcium signal from iodinated vessels, permitting the removal of hard plaques from a CTA scan [95].

In this context, VNCA imaging has been shown to improve the quantification of carotid artery stenoses caused by hard plaques compared to conventional CTA, using digital subtraction angiography as reference [95]. Moreover, lumen assessment did not show to be impacted by blooming artifacts, probably because the algorithm recognizes and removes the spectral behavior of calcium blooming components [95].

### Future outlook

Energy-integrating detectors used in modern DECT platforms are based on an indirect process of x-ray conversion into an electrical signal, which passes by photodiodes and conversion into light photons [96]. On the other hand, new photon-counting detectors directly convert x-ray photons to an electrical signal, increasing dose efficiency and spatial resolution, and improving spectral separation together with its spatial registration. In the near future, photon-counting detector CT platforms may enable not only to visualize BME more in detail, especially in small bones, but also to differentiate among urate crystals, hydroxyapatite, and calcium pyrophosphate deposits [97]. Moreover, preliminary data have shown promising results for subtraction of calcified plaques from vessels, and separation between blood and brain calcifications, overcoming current VNCA limitations of suboptimal material decomposition and resolution restrictions of DECT platforms [98, 99].

However, we are still at the doorstep of this new era of CT technology and further investigation needs to be performed prior to introduction of photon-counting detector CT platforms into clinical routine.

### Conclusions

In the last ten years, DECT-based VNCA imaging has been shown to provide additional clinically relevant information compared to standard CT in several neuroradiology, vascular, and musculoskeletal applications. The greatest experience in using VNCA reconstructions exists in bone marrow imaging to date, particularly for trauma, but also for inflammatory and oncologic bone marrow pathologies. Several studies have demonstrated its potential also for the differentiation of hyperdense lesions as well as for intervertebral disc assessment. In addition, inflammatory or infiltrative bone marrow disorders that are conventionally assessed by means of MRI or bone scintigraphy can be assessed in more detail with DECT in comparison to standard CT. Subjective as well as objective analysis of VNCA images has shown high

diagnostic accuracy and demonstrated its potential to serve as a viable imaging alternative to MRI, bone scintigraphy, or PET/CT in case of contraindications or limited availability. Especially in emergency/trauma settings, patients can substantially benefit from this technique due to time savings, early accurate diagnosis, and prompt therapy initiation. However, despite multiple studies having shown the potential of DECT-based VNCA imaging, this technique still has not gained ground in clinical routine, probably because of its limited availability considering that most of available studies have been performed on second- and third-generation DSCT platforms. This might have limited inter-vendor correlation studies and hampered the integration of VNCA imaging into clinical routine.

It is crucial to be aware of VNCA technical limitations and differences related to acquisition protocols and reconstruction software, which may differ across vendors, and generate different cutoff values for quantitative assessment. Further investigation of VNCA imaging algorithms is needed to gain a more comprehensive understanding of its potential.

### Abbreviations

BME: Bone marrow edema; CTA: Computed tomography angiography; DECT: Dual-energy computed tomography;  $DE_{ratio}$ : Dual-energy ratio; DSCT: Dual-source computed tomography; MRI: Magnetic resonance imaging; HU: Hounsfield units; PET: Positron emission tomography; VNCA: Virtual non-calcium

### Authors' contributions

TD, DC, MHA, and CB have contributed to the design and implementation of the research, to the analysis of the data, and to the writing of the manuscript. All authors have approved the submitted final version of the manuscript and have agreed to be personally accountable for the author's own contributions.

### Funding

Open Access funding enabled and organized by Projekt DEAL.

### Availability of data and materials

Not applicable

### Declarations

#### Ethics approval and consent to participate

Not applicable

#### Consent for publication

Consent for publication has been obtained.

#### Competing interests

MHA received speaking fees from Siemens Healthineers and GE Healthcare. CB received speaking fees from Siemens Healthineers. TA and MHA are members of the *European Radiology Experimental* Editorial Board and they have not taken part in the review or acceptance process of this article. The other authors declare that they have no competing interests.

#### Author details

<sup>1</sup>Department of Biomedical Sciences and Morphological and Functional Imaging, University Hospital Messina, Messina, Italy. <sup>2</sup>Division of Experimental Imaging, Department of Diagnostic and Interventional Radiology, University Hospital Frankfurt, Theodor-Stern-Kai 7, 60590 Frankfurt am Main, Germany.

Received: 15 December 2020 Accepted: 11 June 2021

Published online: 03 September 2021

## References

- D'Angelo T, Cicero G, Mazziotti S et al (2019) Dual energy computed tomography virtual monoenergetic imaging: technique and clinical applications. *Br J Radiol* 92:20180546 <https://doi.org/10.1259/bjr.20180546>
- Lenga L, Lange M, Arendt CT et al (2020) Measurement reliability and diagnostic accuracy of virtual monoenergetic dual-energy CT in patients with colorectal liver metastases. *Acad Radiol* 27:e168–e175 <https://doi.org/10.1016/j.acra.2019.09.020>
- Lenga L, Czwikla R, Wichmann JL et al (2018) Dual-energy CT in patients with abdominal malignant lymphoma: impact of noise-optimised virtual monoenergetic imaging on objective and subjective image quality. *Clin Radiol* 73:833.e19–833.e27. <https://doi.org/10.1016/j.crad.2018.04.015>
- D'Angelo T, Mazziotti S, Ascenti G, Wichmann JL (2017) Miscellaneous and emerging applications of dual-energy computed tomography for the evaluation of pathologies in the head and neck. *Neuroimaging Clin N Am* 27:469–482 <https://doi.org/10.1016/j.nic.2017.04.008>
- Lenga L, Trapp F, Albrecht MH et al (2019) Single- and dual-energy CT pulmonary angiography using second- and third-generation dual-source CT systems: comparison of radiation dose and image quality. *Eur Radiol* 29:4603–4612 <https://doi.org/10.1007/s00330-018-5982-1>
- Arendt CT, Czwikla R, Lenga L et al (2020) Improved coronary artery contrast enhancement using noise-optimised virtual monoenergetic imaging from dual-source dual-energy computed tomography. *Eur J Radiol* 122:108666 <https://doi.org/10.1016/j.ejrad.2019.108666>
- Martin SS, Trapp F, Wichmann JL et al (2019) Dual-energy CT in early acute pancreatitis: improved detection using iodine quantification. *Eur Radiol* 29:2226–2232 <https://doi.org/10.1007/s00330-018-5844-x>
- Lenga L, Albrecht MH, Othman AE et al (2017) Monoenergetic dual-energy computed tomographic imaging: cardiothoracic applications. *J Thorac Imaging* 32:151–158 <https://doi.org/10.1097/RTI.0000000000000259>
- Akisato K, Nishihara R, Okazaki H et al (2020) Dual-energy CT of material decomposition analysis for detection with bone marrow edema in patients with vertebral compression fractures. *Acad Radiol* 27:227–232 <https://doi.org/10.1016/j.acra.2019.02.015>
- Biery G, Venkatasamy A, Kremer S, Dosch JC, Dietemann JL (2014) Dual-energy CT in vertebral compression fractures: performance of visual and quantitative analysis for bone marrow edema demonstration with comparison to MRI. *Skelet Radiol* 43:485–492 <https://doi.org/10.1007/s00256-013-1812-3>
- Burns JE, Yao J, Summers RM (2017) Vertebral body compression fractures and bone density: automated detection and classification on CT images. *Radiology* 284:788–797 <https://doi.org/10.1148/radiol.2017162100>
- Kosmala A, Weng AM, Heideimeier A et al (2018) Multiple myeloma and dual-energy CT: diagnostic accuracy of virtual noncalcium technique for detection of bone marrow infiltration of the spine and pelvis. *Radiology* 286:205–213 <https://doi.org/10.1148/radiol.2017170281>
- Uotani K, Watanabe Y, Higashi M et al (2009) Dual-energy CT head bone and hard plaque removal for quantification of calcified carotid stenosis: utility and comparison with digital subtraction angiography. *Eur Radiol* 19:2060–2065 <https://doi.org/10.1007/s00330-009-1358-x>
- Boks SS, Vroegindewij D, Koes BW, Hunink MGM, Bierma-Zeinstra SMA (2006) Follow-up of occult bone lesions detected at MR imaging: systematic review. *Radiology* 238:853–862 <https://doi.org/10.1148/radiol.2382050062>
- Omoumi P, Becce F, Racine D, Ott JG, Andreisek G, Verdun FR (2015) Dual-energy CT: basic principles, technical approaches and applications in musculoskeletal imaging. *Semin Musculoskelet Radiol* 19:431–437 <https://doi.org/10.1055/s-0035-1569253>
- Peltola EK, Koskinen SK (2015) Dual-energy computed tomography of cruciate ligament injuries in acute knee trauma. *Skelet Radiol* 44:1295–1301 <https://doi.org/10.1007/s00256-015-2173-x>
- Hu R, Daftari Besheli L, Young J et al (2016) Dual-energy head CT enables accurate distinction of intraparenchymal hemorrhage from calcification in emergency department patients. *Radiology* 280:177–183 <https://doi.org/10.1148/radiol.2015150877>
- Nute JL, Le Roux L, Chandler AG, Baladandayuthapani V, Schellingerhout D, Cody DD (2015) Differentiation of low-attenuation intracranial hemorrhage and calcification using dual-energy computed tomography in a phantom system. *Invest Radiol* 50:9–16 <https://doi.org/10.1097/RLI.0000000000000089>
- Wiggins WF, Potter CA, Sodickson AD (2020) Dual-energy CT to differentiate small foci of intracranial hemorrhage from calcium. *Radiology* 294:129–138 <https://doi.org/10.1148/radiol.2019190792>
- Johnson TRC, Krauß B, Sedlmair M et al (2007) Material differentiation by dual energy CT: initial experience. *Eur Radiol* 17:1510–1517 <https://doi.org/10.1007/s00330-006-0517-6>
- Booz C, Hofmann PC, Sedlmair M et al (2017) Evaluation of bone mineral density of the lumbar spine using a novel phantomless dual-energy CT post-processing algorithm in comparison with dual-energy X-ray absorptiometry. *Eur Radiol Exp* 1 <https://doi.org/10.1186/s41747-017-0017-2>
- Primak AN, Ramirez Giraldo JC, Liu X, Yu L, McCollough CH (2009) Improved dual-energy material discrimination for dual-source CT by means of additional spectral filtration. *Med Phys* 36:1359–1369 <https://doi.org/10.1118/1.3083567>
- Liu X, Yu L, Primak AN, McCollough CH (2009) Quantitative imaging of element composition and mass fraction using dual-energy CT: three-material decomposition. *Med Phys* 36:1602–1609 <https://doi.org/10.1118/1.3097632>
- Albrecht M, Vogl T, Martin S et al (2019) Review of clinical applications for virtual monoenergetic dual-energy CT. *Radiology* 293:182297 <https://doi.org/10.1148/radiol.2019182297>
- Lenga L, Leithner D, Peterke JL et al (2019) Comparison of radiation dose and image quality of contrast-enhanced dual-source CT of the chest: single-versus dual-energy and second-versus third-generation technology. *AJR Am J Roentgenol* 212:741–747 <https://doi.org/10.2214/AJR.18.20065>
- Uhrig M, Simons D, Kachelrieß M, Pisana F, Kuchenbecker S, Schlemmer HP (2016) Advanced abdominal imaging with dual energy CT is feasible without increasing radiation dose. *Cancer Imaging* 16:15 <https://doi.org/10.1186/s40644-016-0073-5>
- Wang CK, Tsai JM, Chuang MT, Wang MT, Huang KY, Lin RM (2013) Bone marrow edema in vertebral compression fractures: detection with dual-energy CT. *Radiology* 269:525–533 <https://doi.org/10.1148/radiol.1312577>
- Noguchi K, Itoh T, Naruto N, Takashima S, Tanaka K, Kuroda S (2017) A novel imaging technique (X-Map) to identify acute ischemic lesions using noncontrast dual-energy computed tomography. *J Stroke Cerebrovasc Dis* 26:34–41 <https://doi.org/10.1016/j.jstrokecerebrovasdis.2016.08.025>
- Booz C, Nöske J, Albrecht MH et al (2020) Diagnostic accuracy of color-coded virtual noncalcium dual-energy CT for the assessment of bone marrow edema in sacral insufficiency fracture in comparison to MRI. *Eur J Radiol* 129:109046 <https://doi.org/10.1016/j.ejrad.2020.109046>
- Kelcz F, Joseph PM, Hilal SK (1979) Noise considerations in dual energy CT scanning. *Med Phys* 6:418–425 <https://doi.org/10.1118/1.594520>
- Müller FC, Børgesen H, Gosvig K et al (2019) Optimising dual-energy CT scan parameters for virtual non-calcium imaging of the bone marrow: a phantom study. *Eur Radiol Exp* 3:46 <https://doi.org/10.1186/s41747-019-0125-2>
- Pache G, Krauss B, Strohm P et al (2010) Dual-energy CT virtual noncalcium technique: detecting post-traumatic bone marrow lesions—feasibility study. *Radiology* 256:617–624 <https://doi.org/10.1148/radiol.10091230>
- Wortman JR, Uyeda JW, Fulwadhva UP, Sodickson AD (2018) Dual-energy CT for abdominal and pelvic trauma. *Radiographics* 38:586–602 <https://doi.org/10.1148/rg.2018170058>
- Booz C, Nöske J, Martin SS et al (2019) Virtual noncalcium dual-energy CT: detection of lumbar disk herniation in comparison with standard gray-scale CT. *Radiology* 290:446–455 <https://doi.org/10.1148/radiol.2018181286>
- Suh CH, Yun SJ, Jin W, Lee SH, Park SY, Ryu CW (2019) Diagnostic performance of dual-energy CT for the detection of bone marrow oedema: a systematic review and meta-analysis. *Eur Radiol* 28:4182–4194 <https://doi.org/10.1007/s00330-018-5411-5>
- Jang SW, Chung BM, Kim WT, Gil JR (2019) Nondisplaced fractures on hip CT: added value of dual-energy CT virtual non-calcium imaging for detection of bone marrow edema using visual and quantitative analyses. *Acta Radiol* 60:1465–1473 <https://doi.org/10.1177/028185119831690>
- Kellock TT, Nicolaou S, Kim SSY et al (2017) Detection of bone marrow edema in nondisplaced hip fractures: utility of a virtual noncalcium dual-energy CT application. *Radiology* 284:798–805 <https://doi.org/10.1148/radiol.2017161063>
- Deng H, Zheng W, Jankovic J (2015) Genetics and molecular biology of brain calcification. *Ageing Res Rev* 22:20–38 <https://doi.org/10.1016/j.arr.2015.04.004>
- Martin V, Lemmen LJ (1952) Calcification in intracranial neoplasms. *Am J Pathol* 28:1107–1131
- Chen W, Zhu W, Kovanlikaya I et al (2014) Intracranial calcifications and hemorrhages: characterization with quantitative susceptibility mapping. *Radiology* 270:496–505 <https://doi.org/10.1148/radiol.13122640>

41. Panagos PD, Jauch EC, Broderick JP (2002) Intracerebral hemorrhage. *Emerg Med Clin North Am* 20:631–655 [https://doi.org/10.1016/s0733-8627\(02\)00015-9](https://doi.org/10.1016/s0733-8627(02)00015-9)
42. Tanigawa N, Komemushi A, Kariya S et al (2006) Percutaneous vertebroplasty: relationship between vertebral body bone marrow edema pattern on MR images and initial clinical response. *Radiology* 239:195–200 <https://doi.org/10.1148/radiol.2391050073>
43. Han IH, Chin DK, Kuh SU et al (2009) Magnetic resonance imaging findings of subsequent fractures after vertebroplasty. *Neurosurgery* 64:740–745 <https://doi.org/10.1227/01.NEU.0000339120.41053.F1>
44. Klazen CAH, Lohle PNM, de Vries J et al (2010) Vertebroplasty versus conservative treatment in acute osteoporotic vertebral compression fractures (Vertos II): an open-label randomised trial. *Lancet* 376:1085–1092 [https://doi.org/10.1016/S0140-6736\(10\)60954-3](https://doi.org/10.1016/S0140-6736(10)60954-3)
45. Frellesen C, Azadegan M, Martin SS et al (2018) Dual-energy computed tomography-based display of bone marrow edema in incidental vertebral compression fractures: diagnostic accuracy and characterization in oncological patients undergoing routine staging computed tomography. *Invest Radiol* 53:409–416 <https://doi.org/10.1097/RLI.0000000000000458>
46. Yang P, Wu G, Chang X (2018) Diagnostic accuracy of dual-energy computed tomography in bone marrow edema with vertebral compression fractures: A meta-analysis. *Eur J Radiol* 99:124–129 <https://doi.org/10.1016/j.ejrad.2017.12.018>
47. Guggenberger RC, Gnannt R, Hodler J et al (2012) Diagnostic performance of dual-energy CT for the detection of traumatic bone marrow lesions in the ankle: comparison with MR imaging. *Radiology* 264:164–173 <https://doi.org/10.1148/radiol.12112217>
48. Pache G, Bulla S, Baumann T et al (2012) Dose reduction does not affect detection of bone marrow lesions with dual-energy CT virtual noncalcium technique. *Acad Radiol* 19:1539–1545 <https://doi.org/10.1016/j.jacr.2012.08.006>
49. Yeh BM, Shepherd JA, Wang ZJ, Teh HS, Hartman RP, Prevrhal S (2009) Dual-energy and low-kVp CT in the abdomen. *AJR Am J Roentgenol* 193:47–54 <https://doi.org/10.2214/AJR.09.2592>
50. Flohr TG, McCollough CH, Bruder H et al (2006) First performance evaluation of a dual-source CT (DSCCT) system. *Eur Radiol* 16:256–268 <https://doi.org/10.1007/s00330-005-2919-2>
51. Wang Y, Chen Y, Zheng H, Huang X, Shan C, Bao Y (2020) Detection of different degree traumatic vertebral bone marrow oedema by virtual non-calcium technique of dual-source dual-energy CT. *Clin Radiol* 75:156.e11–156.e19 <https://doi.org/10.1016/j.crad.2019.09.143>
52. Jeong SY, Jeon SJ, Seol M, Ahn TH, Juhng SK (2020) Diagnostic performance of dual-energy computed tomography for detection of acute spinal fractures. *Skeletal Radiol*. <https://doi.org/10.1007/s00256-020-03450-8>
53. Diekhoff T, Engelhard N, Fuchs M et al (2019) Single-source dual-energy computed tomography for the assessment of bone marrow oedema in vertebral compression fractures: a prospective diagnostic accuracy study. *Eur Radiol* 29:31–39 <https://doi.org/10.1007/s00330-018-5568-y>
54. Petritsch B, Kosmala A, Weng AM et al (2017) Vertebral compression fractures: third-generation dual-energy CT for detection of bone marrow edema at visual and quantitative analyses. *Radiology* 284:161–168 <https://doi.org/10.1148/radiol.2017162165>
55. Kaup M, Wichmann JL, Scholtz JE et al (2016) Dual-energy CT-based display of bone marrow edema in osteoporotic vertebral compression fractures: impact on diagnostic accuracy of radiologists with varying levels of experience in correlation to MR imaging. *Radiology* 280:510–519 <https://doi.org/10.1148/radiol.2016150472>
56. Abdullayev N, Große Hokamp N, Lennartz S et al (2019) Improvements of diagnostic accuracy and visualization of vertebral metastasis using multi-level virtual non-calcium reconstructions from dual-layer spectral detector computed tomography. *Eur Radiol* 29:5941–5949 <https://doi.org/10.1007/s00330-019-06233-5>
57. Diekhoff T, Hermann KG, Pumberger M, Hamm B, Putzier M, Fuchs M (2017) Dual-energy CT virtual non-calcium technique for detection of bone marrow edema in patients with vertebral fractures: A prospective feasibility study on a single-source volume CT scanner. *Eur J Radiol* 87:59–65 <https://doi.org/10.1016/j.ejrad.2016.12.008>
58. Foti G, Beltramello A, Catania M, Rigotti S, Serra G, Carboognin G (2019) Diagnostic accuracy of dual-energy CT and virtual non-calcium techniques to evaluate bone marrow edema in vertebral compression fractures. *Radiol Med* 124:487–494 <https://doi.org/10.1007/s11547-019-00998-x>
59. Herman MP, Kopetz S, Bhosale PR et al (2009) Sacral insufficiency fractures after preoperative chemoradiation for rectal cancer: incidence, risk factors, and clinical course. *Int J Radiat Oncol Biol Phys* 74:818–823 <https://doi.org/10.1016/j.ijrobp.2008.08.054>
60. Kushchayev SV, Glushko T, Jarraya M et al (2018) ABCs of the degenerative spin. *Insights Imaging* 9:253–274 <https://doi.org/10.1007/s13244-017-0584-z>
61. Shinohara Y, Sasaki F, Ohmura T, Itoh T, Endo T, Kinoshita T (2020) Evaluation of lumbar intervertebral disc degeneration using dual energy CT virtual non-calcium imaging. *Eur J Radiol* 124:108817 <https://doi.org/10.1016/j.ejrad.2020.108817>
62. van Rijn RM, Wassenaar M, Verhagen AP et al (2012) Computed tomography for the diagnosis of lumbar spinal pathology in adult patients with low back pain or sciatica: a diagnostic systematic review. *Eur Spine J* 21:228–239 <https://doi.org/10.1007/s00586-011-2012-2>
63. Notohamiprodjo S, Stahl R, Braunagel M et al (2017) Diagnostic accuracy of contemporary multidetector computed tomography (MDCT) for the detection of lumbar disc herniation. *Eur Radiol* 27:3443–3451 <https://doi.org/10.1007/s00330-016-4686-7>
64. Abeloff MD, Armitage JO, Niederhuber JE, Kastan MB, McKenna WG (2008) *Abeloff's Clinical Oncology*, 4th edn. Churchill Livingstone Elsevier, Philadelphia, Pa, USA
65. Yang HL, Liu T, Wang XM, Xu Y, Deng SM (2011) Diagnosis of bone metastases: a meta-analysis comparing <sup>18</sup>F-FDG PET, CT, MRI and bone scintigraphy. *Eur Radiol* 21:2604–2617 <https://doi.org/10.1007/s00330-011-2221-4>
66. Kosmala A, Weng AM, Krauss B, Knop S, Bley TA, Petritsch B (2018) Dual-energy CT of the bone marrow in multiple myeloma: diagnostic accuracy for quantitative differentiation of infiltration patterns. *Eur Radiol* 28:5083–5090 <https://doi.org/10.1007/s00330-018-5537-5>
67. Wang Q, Sun Z, Li S et al (2017) Bone marrow imaging by third-generation dual-source dual-energy CT using virtual noncalcium technique for assessment of diffuse infiltrative lesions of multiple myeloma. *Zhongguo Yi Xue Ke Xue Yuan Xue Bao* 39:114–119 <https://doi.org/10.3881/j.issn.1000-503X.2017.01.019>
68. Ensrud KE (2013) Epidemiology of fracture risk with advancing age. *J Gerontol A Biol Sci Med Sci* 68:1236–1242 <https://doi.org/10.1093/gerona/glt092>
69. Reddy T, McLaughlin PD, Mallinson PI et al (2015) Detection of occult, undisplaced hip fractures with a dual-energy CT algorithm targeted to detection of bone marrow edema. *Emerg Radiol* 22:25–29 <https://doi.org/10.1007/s10140-014-1249-6>
70. Wu H, Zhang G, Shi L et al (2019) Axial spondyloarthritis: dual-energy virtual noncalcium CT in the detection of bone marrow edema in the sacroiliac joints. *Radiology* 290:157–164 <https://doi.org/10.1148/radiol.2018181168>
71. Chen M, Herregods N, Jaremko JL et al (2020) Bone marrow edema in sacroiliitis: detection with dual-energy CT. *Eur J Radiol* 30:3393–3400 <https://doi.org/10.1007/s00330-020-06670-7>
72. Jans L, De Kock I, Herregods N et al (2018) Dual-energy CT: a new imaging modality for bone marrow oedema in rheumatoid arthritis. *Ann Rheum Dis* 77:958–960 <https://doi.org/10.1136/annrheumdis-2018-213152>
73. Guggenberger R (2019) Dual-energy CT in the detection of bone marrow edema in the sacroiliac joints: is there a case for axial spondyloarthritis? *Radiology* 290:165–166 <https://doi.org/10.1148/radiol.2018182224>
74. Foti G, Faccioli N, Silva R, Oliboni E, Zorzi C, Carboognin G (2020) Bone marrow edema around the hip in non-traumatic pain: dual-energy CT vs MRI. *Eur Radiol* 30:4098–4106 <https://doi.org/10.1007/s00330-020-06775-z>
75. Burke MC, Garg A, Youngner JM, Deshmukh SD, Omar IM (2019) Initial experience with dual-energy computed tomography-guided bone biopsies of bone lesions that are occult on monoenergetic CT. *Skeletal Radiol* 48:605–613 <https://doi.org/10.1007/s00256-018-3087-1>
76. Mallee WH, Wang J, Poolman RW et al (2015) Computed tomography versus magnetic resonance imaging versus bone scintigraphy for clinically suspected scaphoid fractures in patients with negative plain radiographs. *Cochrane Database Syst Rev*:CD010023 <https://doi.org/10.1002/14651858.CD010023>
77. Peh WC, Gilula LA, Wilson AJ (1996) Detection of occult wrist fractures by magnetic resonance imaging. *Clin Radiol* 51:285–292 [https://doi.org/10.1016/s0009-9260\(96\)80348-5](https://doi.org/10.1016/s0009-9260(96)80348-5)
78. Newton EJ, Love J (2007) Emergency department management of selected orthopedic injuries. *Emerg Med Clin North Am* 25:763–793 <https://doi.org/10.1016/j.emc.2007.07.003>
79. Markhardt BK, Gross JM, Monu JUV (2009) Schatzker Classification of Tibial Plateau Fractures: Use of CT and MR Imaging Improves Assessment. *Radiographics* 29:585–597 <https://doi.org/10.1148/rg.292085078>
80. Wang MY, Zhang XY, Xu L et al (2019) Detection of bone marrow edema in knee joints using a dual-energy CT virtual non-calcium technique. *Clin Radiol* 74:815.e1–815.e7 <https://doi.org/10.1016/j.crad.2019.06.020>

81. Yang SJ, Jeon JY, Lee SW, Jeong YM (2020) Added value of color-coded virtual non-calcium dual-energy CT in the detection of acute knee fractures in non-radiology inexperienced readers. *Eur J Radiol* 129:109112 <https://doi.org/10.1016/j.ejrad.2020.109112>
82. Booz C, Nöske J, Lenga L et al (2020) Color-coded virtual non-calcium dual-energy CT for the depiction of bone marrow edema in patients with acute knee trauma: a multireader diagnostic accuracy study. *Eur Radiol* 30:141–150 <https://doi.org/10.1007/s00330-019-06304-7>
83. Yadav H, Khanduri S, Yadav P, Pandey S, Yadav VK, Khan S (2020) Diagnostic accuracy of dual energy CT in the assessment of traumatic bone marrow edema of lower limb and its correlation with MRI. *Indian J Radiol Imaging* 30:59–63 [https://doi.org/10.4103/ijri.IJRI\\_59\\_19](https://doi.org/10.4103/ijri.IJRI_59_19)
84. Dareez NM, Dahlslett KH, Engesland E, Lindland ES (2017) Scaphoid fracture: bone marrow edema detected with dual-energy CT virtual non-calcium images and confirmed with MRI. *Skeletal Radiol* 46:1753–1756 <https://doi.org/10.1007/s00256-017-2730-6>
85. Booz C, Nöske J, Albrecht MH et al (2019) Traumatic bone marrow edema of the calcaneus: evaluation of color-coded virtual non-calcium dual-energy CT in a multi-reader diagnostic accuracy study. *Eur J Radiol* 118:207–214 <https://doi.org/10.1016/j.ejrad.2019.07.023>
86. Ali IT, Wong WD, Liang T et al (2018) Clinical utility of dual-energy CT analysis of bone marrow edema in acute wrist fractures. *AJR Am J Roentgenol* 210:842–847 <https://doi.org/10.2214/AJR.17.18673>
87. Foti G, Catania M, Caia S et al (2019) Identification of bone marrow edema of the ankle: diagnostic accuracy of dual-energy CT in comparison with MRI. *Radiol Med* 124:1028–1036 <https://doi.org/10.1007/s11547-019-01062-4>
88. Koch V, Müller FC, Gosvig K et al (2021) Incremental diagnostic value of color-coded virtual non-calcium dual-energy CT for the assessment of traumatic bone marrow edema of the scaphoid. *Eur Radiol*. <https://doi.org/10.1007/s00330-020-07541-x>
89. Mallinson PI, Stevens C, Reisinger C, Nicolaou S, Munk PL, Ouellette H (2013) Achilles tendinopathy and partial tear diagnosis using dual-energy computed tomography collagen material decomposition application. *J Comput Assist Tomogr* 37:475–477 <https://doi.org/10.1097/RCT.0b013e318287efa0>
90. Hachamovitch R, Nutter B, Hlatky MA et al (2012) SPARC investigators, patient management after noninvasive cardiac imaging results from SPARC (Study of myocardial perfusion and coronary anatomy imaging roles in coronary artery disease). *J Am Coll Cardiol* 59:462–474 <https://doi.org/10.1016/j.jacc.2011.09.066>
91. Lell MM, Ditt H, Panknin C et al (2007) Bone-subtraction CT angiography: evaluation of two different fully automated image-registration procedures for interscan motion compensation. *AJNR Am J Neuroradiol* 28:1362–1368 <https://doi.org/10.3174/ajnr.A0558>
92. Tabari A, Gee MS, Singh R et al (2020) Reducing radiation dose and contrast medium volume with application of dual-energy CT in children and young adults. *AJR Am J Roentgenol* 214:1199–1205 <https://doi.org/10.2214/AJR.19.22231>
93. D'Angelo T, Lenga L, Arendt CT et al (2020) Carotid and cerebrovascular dual-energy computed tomography angiography: Optimization of window settings for virtual monoenergetic imaging reconstruction. *Eur J Radiol* 130:109166 <https://doi.org/10.1016/j.ejrad.2020.109166>
94. Leithner D, Mahmoudi S, Wichmann JL et al (2018) Evaluation of virtual monoenergetic imaging algorithms for dual-energy carotid and intracerebral CT angiography: Effects on image quality, artefacts and diagnostic performance for the detection of stenosis. *Eur J Radiol* 99:11–117 <https://doi.org/10.1016/j.ejrad.2017.12.024>
95. Mannil M, Ramachandran J, Vittoria de Martini I et al (2017) Modified dual-energy algorithm for calcified plaque removal: evaluation in carotid computed tomography angiography and comparison with digital subtraction angiography. *Invest Radiol* 52:680–685 <https://doi.org/10.1097/RLI.0000000000000391>
96. Alkadhi H, Euler A (2020) The future of computed tomography: personalized, functional, and precise. *Invest Radiol* 55:545–555 <https://doi.org/10.1097/RLI.0000000000000668>
97. Stamp LK, Anderson NG, Becce F et al (2019) Clinical utility of multi-energy spectral photon-counting computed tomography in crystal arthritis. *Arthritis Rheumatol* 71:1158–1162 <https://doi.org/10.1002/art.40848>
98. Riederer I, Si-Mohamed S, Ehn S et al (2019) Differentiation between blood and iodine in a bovine brain-initial experience with spectral photon-counting computed tomography (SPCCT). *PLoS One* 14:e0212679 <https://doi.org/10.1371/journal.pone.0212679>
99. Sartoretti T, Eberhard M, Rüschoff JH et al (2020) Photon-counting CT with tungsten as contrast medium: experimental evidence of vessel lumen and plaque visualization. *Atherosclerosis*. 310:11–16 <https://doi.org/10.1016/j.atherosclerosis.2020.07.023>

## Publisher's Note

Springer Nature remains neutral with regard to jurisdictional claims in published maps and institutional affiliations.

**Submit your manuscript to a SpringerOpen<sup>®</sup> journal and benefit from:**

- Convenient online submission
- Rigorous peer review
- Open access: articles freely available online
- High visibility within the field
- Retaining the copyright to your article

---

Submit your next manuscript at ► [springeropen.com](https://www.springeropen.com)

---